A global hybrid model for Mercury's interaction with the solar wind: Case study of the dipole representation

Emilie Richer, Ronan Modolo, Gérard Chanteur, Sebastien Hess, François Leblanc

A global hybrid model for Mercury's interaction with the solar wind: Case study of the dipole representation

E. Richer,[1] R. Modolo,[2] G. M. Chanteur,[3] S. Hess,[2] and F. Leblanc[4]

Received 2 May 2012; revised 10 September 2012; accepted 10 September 2012; published 25 October 2012.

[1] The interaction of the solar wind (SW) with the magnetic field of Mercury is investigated by means of a three dimensional parallelized multispecies hybrid model. A comparison between two mathematical representations of Mercury's intrinsic magnetic field is studied. The first model is an Offset Dipole (OD) having the offset and dipolar moment reported by Anderson et al. (2011). The second model is a combination of a Dipole and a Quadrupole (DQ), the total field is fitted to the offset dipolar field, for northern latitudes greater than 50°. Simulations reproduce the features which characterize Mercury's interaction with the SW, encompassing the Bow Shock (BS), the magnetosheath, the magnetotail, the "cusps" region and the neutral current sheet. Global hybrid simulations of the Hermean magnetosphere run for the OD and DQ models demonstrate that the southern parts of the magnetospheres produced by the OD and DQ models differ greatly in topology and volume meanwhile their northern parts-are quite similar. In particular the DQ model exhibits a dome of closed field lines around the south pole in contrast to the OD. Without further information on the intrinsic magnetic field of the planet in the southern region which should be provided by BepiColombo after year 2020, we can only speculate on the influence of the different magnetic topologies on the magnetospheric dynamics.

Citation: Richer, E., R. Modolo, G. M. Chanteur, S. Hess, and F. Leblanc (2012), A global hybrid model for Mercury's interaction with the solar wind: Case study of the dipole representation, *J. Geophys. Res.*, *117*, A10228, doi:10.1029/2012JA017898.

1. Introduction

[2] Mariner 10 flybys revealed a substantial intrinsic magnetic field, a small but highly time-variable magnetosphere and a detached Bow Shock (BS) [*Ness et al.*, 1975; *Ogilvie et al.*, 1977; *Russell et al.*, 1988]. A preliminary study of magnetometer data from Mariner 10 first flyby inferred the presence of a magnetic dipole [*Ness et al.*, 1974]. Magnetic field data were interpreted using a spherical harmonic development in order to obtain a multipolar decomposition of the observed field up to the second order [*Ness et al.*, 1975, 1976]. This analysis suggested a centered dipole representation of Mercury's intrinsic magnetic field and established constraints on its dipole moment. Higher order multipoles were associated to external sources (contributions from magnetosheath and plasma sheet currents). MESSENGER observations during the three flybys of Mercury brought additional information and set on the front page the investigation of the structure and the origin of Mercury's magnetic field. The first MESSENGER flyby leads to an estimate of the dipolar moment equal to 230–290 nT $\times$ R_M^3, 1/100 of Earth's dipolar moment, and a non-dipolar contribution corresponding at most to 52% of the dipole field [*Anderson et al.*, 2008]. *Alexeev et al.* [2010] have used a paraboloidal model combined with an Offset Dipole (OD) representation proposed by *Ness et al.* [1974] to compute Mercury's magnetospheric field during MESSENGER flybys. A dipole moment of 196 nT $\times$ R_M^3 with a Northward offset of 405 km resulted from this investigation. Since the orbital insertion, of MESSENGER on March 18th 2011, investigations of Mercury's intrinsic magnetic field have been carried further and *Anderson et al.* [2011] reached the conclusion that a northward shifted dipole with a northward offset equal to 484 $\pm$ 11 km and a dipolar moment of 195 nT $\times$ R_{ME}^3 provides a good approximation in the light of MESSENGER observations at northern latitudes higher than 30°. *Anderson et al.* [2011] also emphasized that the observed field is well represented by combined dipolar and quadrupolar terms in a spherical harmonic analysis of MESSENGER magnetic field data above 30°N.

[3] In addition, Mariner 10 observations enlightened the absence of substantial atmosphere and ionosphere but an upper limit of exospheric species such H, He and O, have

[1]Laboratoire de Physique des Plasmas, UPMC, Ecole Polytechnique, Palaiseau, France.
[2]LATMOS, UVSQ, IPSL, Guyancourt, France.
[3]Laboratoire de Physique des Plasmas, Ecole Polytechnique, Palaiseau, France.
[4]LATMOS, IPSL, CNRS, Paris, France.

Corresponding author: E. Richer, Laboratoire de Physique des Plasmas, UPMC, Ecole Polytechnique, Route de Saclay, FR-91128 Palaiseau, France. (emilie.richer@lpp.polytechnique.fr)

0148-0227/12/2012JA017898

been deduced [*Broadfoot et al.*, 1976]. Ground based observations demonstrated that Mercury has a very changing exosphere and additional exospheric components, Na, K and Ca, were identified [*Potter and Morgan*, 1985, 1986; *Bida et al.*, 2000; *Leblanc et al.*, 2006]. MESSENGER flybys refined the knowledge of Mercury's exosphere, confirmed the highly asymmetrical distributions of Na and Ca around Mercury and revealed the presence of Mg in the exosphere [*McClintock et al.*, 2008, 2009]. Na observations show a stronger emission near the poles of Mercury while Ca emission increases from dusk to dawn [*McClintock et al.*, 2008]. The distribution of exospheric components is related to processes that supply and deplete the exosphere. Since Mercury's exobase coincides with the surface of the planet, a part of the exosphere originates from the extraction of atoms from the surface. Extraction processes due to Solar Wind (SW) sputtering, thermal and photon stimulated desorptions and micrometeoroid impacts are described by *Killen et al.* [2007].

[4] Mercury's exosphere and magnetosphere are strongly dependent since the exosphere ionization is a source of planetary ions which supply Mercury's magnetosphere [*Killen et al.*, 2007; *Zurbuchen et al.*, 2008, 2011]. MESSENGER reported on the plasma composition in Mercury's vicinity and emphasized the presence of ionized exospheric populations such Na^+, K^+ and O^+, to mention only them [*Zurbuchen et al.*, 2008; *Slavin et al.*, 2008; *Raines et al.*, 2011].

[5] In addition to observations, meaningful efforts of modeling have been lead on Mercury. Numerical simulations offer a global description of the SW interaction with Mercury, allow setting back in situ measurements in a three dimensional context and help to separate temporal from spatial fluctuations. Magnetohydrodynamic and hybrid simulations have been performed to simulate Mercury's interaction with the SW.

[6] Hybrid simulations of *Trávníček et al.* [2007] highlighted variations of the position of the BS with SW pressure by testing low and high pressure cases in order to mimic SW conditions at Mercury's aphelion and perihelion. This study leads in particular to a very small stand-off distance of the SW in the high pressure case. The role of the Interplanetary Magnetic Field (IMF) direction in determining the structure of the magnetosphere has been investigated by *Kallio and Janhunen* [2004] and *Trávníček et al.* [2010]. *Trávníček et al.* [2010] highlight substantial differences, especially for the position of the BS and the magnetospheric configuration, between purely northward and southward IMF cases. Hybrid simulations using the IMF orientations of the first (northward IMF) and second (southward IMF) flybys of MESSENGER and the SW plasma parameters at Mercury's aphelion were performed by *Wang et al.* [2010] and, with an adaptative model, by *Müller et al.* [2011]. As *Trávníček et al.* [2010], these studies emphasized important differences between the results given by the two configurations of the IMF. A general conclusion from numerical investigations stressed that the Hermean magnetosphere is affected by external conditions and, due to its compact size, responds quickly to changes of the interplanetary environment [*Fujimoto et al.*, 2007]. Such fast magnetospheric reconfigurations are supported by MESSENGER flybys plasma observations [*Raines et al.*, 2011].

[7] Due to the lack of an ionosphere, the conductivity of the planetary surface plays a crucial role in the closure of the currents system. The effects of surface conductivity models were investigated by *Janhunen and Kallio* [2004], and magnetospheric asymmetries were pointed out. The intrinsic magnetic field is an important driver of the nature of the SW/Mercury interaction but the lack of low altitude observations of the magnetic field above the southern hemisphere of Mercury does not allow definitive conclusions about the topology of the planetary magnetic field. *Kabin et al.* [2008] performed MHD simulations with different sources of Mercury's magnetic field comparing a tilted dipolar magnetic field with a tilted dipolar and quadrupolar magnetic field. Valuable information can be deduced on the internal structure of Mercury by studying its magnetosphere and trying to separate for internal and external contributions to magnetic fields observations by MESSENGER. However, the ever changing interplanetary conditions induce a variability of the magnetospheric field which could be of the same order as differences between models of the planetary field making their discrimination uncertain. MESSENGER orbits for which solar wind and IMF conditions do not change significantly while the satellite is crossing the magnetosphere can be used for an accurate determination of the internal field [*Kabin et al.*, 2008]. They investigate the multipole development of Mercury's intrinsic magnetic field and quantify the external magnetic field. This study supports a multipole representation with both dipole and non-dipole terms for Mercury's magnetic field. *Vogt et al.* [2004, 2007] have shown that large scale current systems and magnetic field topology of quadrupolar magnetospheres have a considerable influence on the global magnetospheric configuration.

[8] The present study aims first, to investigate the interaction of Mercury's intrinsic magnetic field with the SW by the means of hybrid simulation and second, to establish the sensitivity of the global interaction upon the representation of the Hermean internal field. Two representations of the internal magnetic field are tested: 1/ a northward OD, according to *Anderson et al.* [2011], 2/ a combination of a centered DQ fitted to the OD in order to comply with MESSENGER observations above 50°N latitudes. The hybrid model used to perform the simulations and models of intrinsic magnetic field are described in section 2 while the simulation results are presented and discussed in sections 3 and 4.

2. Simulations

2.1. The Hybrid Model

[9] The model used in this study adopts a so-called hybrid formalism where fully kinetic description is applied to ions meanwhile electrons are treated as mass less fluid which ensures the charge neutrality of the plasma and contributes to the total current and pressure. This hybrid model is based on the CAM-CL algorithm [*Matthews*, 1994] and is adapted version of the Martian and Titan simulation models [*Modolo et al.*, 2005; *Modolo and Chanteur*, 2008]. The present model has been parallelized and adapted to describe the SW interaction with the Hermean magnetosphere. The present study does not require a kinetic treatment but we use the hybrid simulation model and program that we are presently

Table 1. Mean Values and Standard Deviations of the Inbound and Outbound IMF Intensity and Components Observed by MESSENGER on April 23, 2011[a]

Parameters	Inbound (nT)	Outbound (nT)
$B_{IMF,X}$	-5.9 ± 1.8	-2.4 ± 2.0
$B_{IMF,Y}$	16.5 ± 2.0	12.1 ± 1.3
$B_{IMF,Z}$	2.4 ± 3.0	-0.3 ± 1.7

[a]Inbound parameters are computed from 16:00 to 17:00 and outbound parameters, from 20:20 to 21:00.

developing in order to investigate general plasma processes around Mercury where kinetic effects cannot be ignored.

[10] The coordinate system used is the following: the x axis corresponds to the Sun-Mercury direction (the SW flows in the +X direction), the Z axis is positive normal to the orbital plane (the magnetic dipole moment of Mercury's intrinsic field points in the –Z direction) and the y axis completes the right-handed system. The simulation is performed in a three dimensional box with $186 \times 400 \times 400$ mesh nodes equally spaced by $\Delta = 3\ c/\omega_{pi} \cong 120$ km, where c/ω_{pi} is the ion inertia length of undisturbed SW protons. The computational domain is thus limited to $-4.5\ R_M < X < +4.5\ R_M$, $-9.8\ R_M < Y, Z < +9.8\ R_M$ with R_M being Mercury's radius.

[11] The time step equals to $0.05\Omega_{ci}^{-1} = 2.5 \times 10^{-2}$ s, where Ω_{ci} is the proton gyrofrequency of the undisturbed SW. A steady state is reached after about three crossing times of the SW through the simulation domain which corresponds to 6000 time steps.

[12] The SW plasma is injected in the YZ plane at $X = -4.5\ R_M$ (entry face of the simulation) with a Maxwellian velocity distribution and exits freely in the YZ at $X = +4.5\ R_M$ (exit plane). The IMF and the motional electric field ($\boldsymbol{E} = -\boldsymbol{v} \times \boldsymbol{B}$) are imposed at the entry face (Neuman conditions) while open/free boundaries (zero gradient) are set in the exit plane (Dirichlet conditions). Periodic conditions are applied to lateral faces for both particles and electromagnetic fields. The outer crust and mantle conductivities are poorly constrained by observations or models. Assuming that the Hermean regolith and mantle have similar electric properties than the Moon leads to conductivity values ranging from 10^{-9} Sm^{-1} to 10^{3} Sm^{-1} [*Glassmeier*, 1997], resulting in variations of the height-integrated conductivity over six decades ($\Sigma = 0.05 - 50000$ S). Under these circumstances, no conductivity terms are setup in the obstacle but the Hermean intrinsic magnetic field is imposed at each time step inside the obstacle (from 0.75 R_M to the surface). Particles impacting the planet are stopped in the obstacle leading to zero ion velocity.

2.2. The Simulation Parameters

[13] The simulation model includes two ion species: SW protons and alpha particles with respective percentages of 95% and 5%. Planetary ions are not modeled in this study and therefore we assume that the contribution of planetary plasma to the current is negligible.

[14] The simulation has been performed with a realistic set of SW plasma parameters at Mercury's aphelion: a plasma density of 32 cm^{-3}, a proton temperature of 11.2 eV (and 44.8 eV for alpha particles) and a bulk speed of 430 km/s [*Milillo et al.*, 2005].

[15] The IMF used in this study is fixed by MESSENGER magnetic fields observations acquired on April 23, 2011. The IMF is set to: (6;−13;0) nT. Although the IMF orientation is unusual, since it differs significantly from the average orientation defined by the Parker Spiral, it has two main advantages. First, it has no component in the +Z direction which is interesting to investigate the north-south asymmetry of the BS and the Hermean magnetosphere. Second, the IMF is quite stable with almost identical components in the inbound and outbound pass: the average values and standard deviations of inbound and outbound magnetic field components are presented in Table 1.

2.3. The Intrinsic Magnetic Field Models

[16] Two simulations have been performed with different models of the intrinsic magnetic field: an OD and the combination of a dipole and a quadrupole (DQ).

[17] The first simulation (SIMU1) is completed with a northward (+Z) OD of 484 km with respect to the center of the planet and with a magnetic moment which equals $\boldsymbol{m}_d = -196\ \text{nT} \times R_M^3 \boldsymbol{e}_z$, in agreement with MESSENGER observations [*Anderson et al.*, 2011].

[18] In this approximation, the intrinsic magnetic field is expressed as $\boldsymbol{B_d}(\boldsymbol{r} - \boldsymbol{r_c})$, where $\mathbf{r_c}$ is the vector position of the center of the shifted dipole, the dipolar field being given by

$$\boldsymbol{B_d}(\boldsymbol{r}) = \frac{\mu_0}{4\pi\|\boldsymbol{r}\|^3}\left(3\frac{\boldsymbol{r}[\boldsymbol{m_d}.\boldsymbol{r}]}{\|\boldsymbol{r}\|^2} - \boldsymbol{m_d}\right),$$

The second simulation (SIMU2) involves a combination of centered dipolar and quadrupolar fields (DQ), which is the beginning of the multipolar development of the magnetic field. The respective contributions of the magnetic dipole and quadrupole are weighted by coefficients c_d and c_q. The resulting magnetic field can be written in the following form:

$$\boldsymbol{B_{dq}}(\boldsymbol{r}, c_d, c_q) = c_d \boldsymbol{B_d}(\boldsymbol{r}) + c_q \boldsymbol{B_q}(\boldsymbol{r}).$$

The quadrupolar field $\boldsymbol{B_q}$ is expressed as:

$$\boldsymbol{B_q}(\boldsymbol{r}) = \frac{\mu_0}{4\pi\|\boldsymbol{r}\|^5}\left(5\frac{\boldsymbol{r}\boldsymbol{r}^t}{\|\boldsymbol{r}\|^2} - 2I\right)\boldsymbol{Q}\boldsymbol{r},$$

Where $\boldsymbol{Q}$ is the quadrupolar moment tensor, with $Q_0 = 196\ \text{nT} \times R_M^4$:

$$\boldsymbol{Q} = Q_0\begin{pmatrix} 1 & 0 & 0 \\ 0 & 1 & 0 \\ 0 & 0 & -2 \end{pmatrix}.$$

Due to its highly eccentric polar orbit with a periapsis located near the north geographic pole, MESSENGER explores the Hermean magnetosphere at altitudes low enough to analyze the source of the planetary magnetic field in the northern hemisphere. But this bias of the orbital coverage restrains comparisons between observations and models to sufficiently high northern latitudes. Here c_d and c_q coefficients are adjusted to produce a resulting magnetic field $\boldsymbol{B_{dq}}$ comparable to the shifted dipole approximation for northern latitudes higher than 50°.

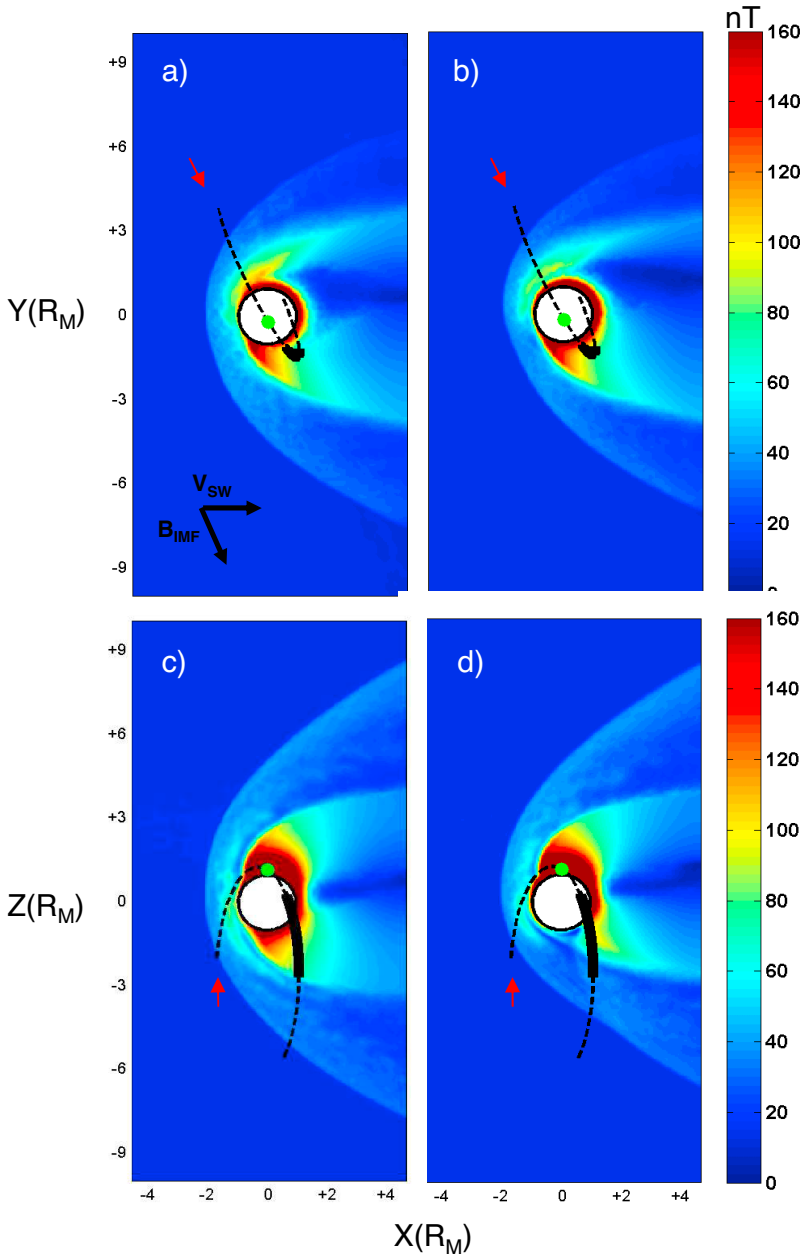

Figure 1. Magnetic field magnitude (in nT) mapped in (a and b) the XY plane and (c and d) the XZ plane, for SIMU1 (Figures 1a and 1c) and SIMU2 (Figures 1b and 1d). In each figure, Mercury is represented by the white disk and the projections of MESSENGER trajectory of April 23, 2011 are over plotted on the maps (black dashed lines). The green dot represents the projection of the Closest Approach position and the portion of MESSENGER trajectory corresponding to the time interval between 18:20 UTC and 19:10 UTC is represented by the black bold solid line. The beginning of MESSENGER trajectory is represented by the red arrow. The directions of the IMF and of the SW bulk velocity are indicated in Figure 1a.

[19] The dipolar and quadrupolar contributions to the total field are determined by the least squares method leading to c_d and c_q coefficients equal to 0.72 and 0.38.

3. Results

3.1. Global Results

[20] The main features of the three-dimensional magnetic field draping around Mercury can be discussed by examining two-dimensional cuts of the simulation domain. Figure 1 is composed of four panels displaying maps of the total magnetic computed from SIMU1 and SIMU2. Figures 1a and 1b display the solution in the XY plane for SIMU1 and SIMU2 (this plane contains the SW and the IMF directions) while Figures 1c and 1d present Btot in the XZ plane (respectively for SIMU1 and SIMU2). Figure 1 shows the deformation of the intrinsic magnetic field caused by its interaction with the SW; this is also visible on the representation of the magnetic

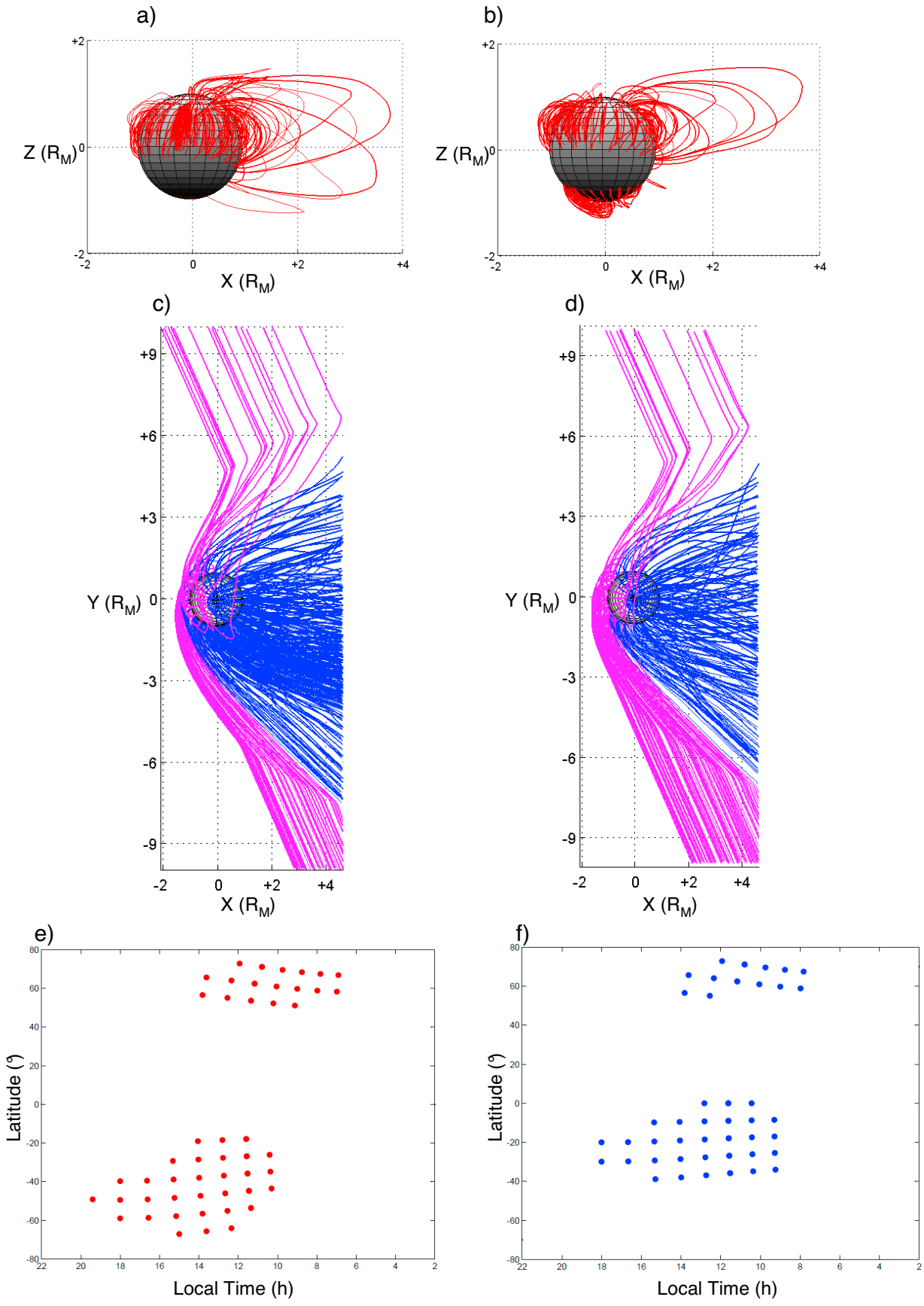

Figure 2

Table 2. Parameters L and ε and Additional Characteristics of the Conic Sections Representing the BS[a]

Source	L (R_M)	E	X_0 (R_M)	L_X (R_M)
Moldovan et al. [2011]	2.7	1.07	+0.5	1.3
Slavin et al. [2009]	2.4	1.07	+0.5	1.16
SIMU1 (XY plane, XZ plane)	4.3, 4.5	0.92, 1.05	0	2.2
SIMU2 (XY plane, XZ plane)	4.1, 4.1	0.9, 1	0	~2.1

[a]X_0 and L_X correspond respectively to the conic section center distance and the SW stand-off distance to the planet center. For each simulation the fits are different in the XY plane and in the XZ plane: the simulated BS is not exactly cylindrically symmetrical. *Moldovan et al.* [2011] calculations take into account an offset along the Z axis of +0.2RM which is not indicated in the table.

field lines on Figure 2. Different boundaries and regions can be identified in simulation results such as the BS, the magnetopause (MP), the magnetosheath, the magnetotail, the cross tail current sheet and the magnetic "cusps."

[21] Figure 2 shows the magnetic field lines corresponding to the simulated magnetic field for SIMU1 (Figures 2a and 2c) and SIMU2 (Figures 2b and 2d). Closed field lines are represented in red in Figures 2a and 2b in the XZ plane and open field lines are represented in the XY plane. Note that two types of open field lines appear on Figures 2c and 2d, open field lines clearly connected to the IMF are represented in magenta and field lines that are neither connected to the IMF nor closed in the tail are represented in blue. Due to the finite size of the simulated domain there are four types of magnetic field lines: *i*/ IMF lines just cross the simulation domain from one face to another one, they are not tied to the planet, ii/ field lines having one end on the planet and having near the other end a rectilinear segment parallel to the undisturbed IMF upstream of the BS, they can be identified as reconnected open field lines and they present an angular point at their crossing of the BS, *iii*/ field lines tied to the planet at both extremities which are clearly closed magnetospheric field lines, *iv*/ last there are field lines connected to the planet at one end only and crossing a boundary face of the simulation domain without having crossed the BS, these lines are either closed magnetospheric field lines or open field line connected to the IMF but there is no way to discriminate these two possibilities without enlarging the simulation domain. Field lines of the fourth type will not be discussed further and are not considered in the following discussion. Such uncertainty about the closure or the connection to the IMF of the field lines arises because of the limited size of the simulation domain.

[22] The feet of the reconnected field lines feet are plotted on Figures 2e and 2f and give an indication of the position of the "cusps." In terrestrial magnetospheric physics the cusps are regions located inside the nominal magnetopause and filled by magnetosheath like plasma [*Cargill et al.*, 2005]. These regions encompass open field lines connected to the IMF on the dayside. These regions correspond also to large precipitating fluxes of SW protons resulting in efficient production of exospheric Na atoms by sputtering of the planetary surface. "Cusps" are located in both northern and southern hemispheres. The largest "cusp" region is present on the southern hemisphere for both simulations. Modeling efforts showed that the location and size of the "cusps" are driven by the IMF direction [*Massetti et al.*, 2003, 2007; *Kallio and Janhunen*, 2004; *Trávníček et al.*, 2007]. *Potter et al.* [2006] reported observations of Na in polar region hypothetically extracted from the surface by SW ions sputtering [*Potter and Morgan*, 1990], Na excess was observed either in the northern or in the southern hemisphere depending on the SW configuration allowing SW ions impact on the surface. *Leblanc et al.* [2009] present ground based observations of Mercury's Na exosphere with the telescope THEMIS and observed peaks of Na emission in both hemispheres but stronger in the southern hemisphere.

[23] SIMU1 and SIMU2 present large similarities in the Northern hemisphere (+Z hemisphere, Figures 1c and 1d and Figures 2e and 2f), locations of BS, MP and "cusps" are comparable. In the equatorial plane (Figures 1a and 1b), the situation is equivalent although a stronger magnetic field is noticed very close to the planet for SIMU2. This difference is mainly due to the centered dipole contribution which is more intense at Z = 0 than the shifted dipole. Closed field lines are mainly present in the northern hemisphere (Figures 2a and 2b).

[24] The situation is drastically different in the Southern hemisphere (−Z hemisphere). SIMU1 results emphasize a larger magnetosphere and the shock is more extended than in SIMU2. The mathematical representation of the dipolar and quadrupolar field induces a magnetic dome of closed field lines near the South Pole (Figure 2b). "Cusps" are larger in SIMU2 and extend to lower latitudes than in SIMU1.

[25] The average BS position, deduced from observations, is usually represented by a conic section with cylindrical symmetry with respect to the Sun-Mercury axis. It is modeled by a formula [*Russell*, 1977; *Slavin and Holzer*, 1981]:

$$r_{BS} = \frac{L}{1 + \varepsilon \cos(\theta_{BS})};$$

r_{BS} and θ_{BS} are the polar coordinates, L is the distance to the BS in the focus plane (taken here to contain the center of the planet) and ε its eccentricity.

[26] Parameters of the conic sections corresponding to MESSENGER observations [*Slavin et al.* 2009; *Moldovan et al.*, 2011] and simulations are listed in Table 2. It has to be noticed that *Moldovan et al.* [2011, Figure 3] show a large dispersion of BS crossings. Some characteristics of the conic sections appear in Table 2 where L_X corresponds to the SW stand-off distance and X_0 the focus of the conic. The average stand-off distances determined for the Hermean BS are very close to the Martian BS characteristic values (about 1.6 Martian radii [*Vignes et al.*, 2000]) and significantly smaller than that of the Terrestrial BS (about 13 Terrestrial radii [*Slavin and Holzer*, 1981]).

Figure 2. Magnetic field lines. Closed field lines are represented in the XZ plane for (a) SIMU1 and (b) SIMU2. Open field lines are represented in the XY plane for (c) SIMU1 and (d) SIMU2. Open field lines clearly connected to the IMF are colored in magenta; the others are colored in blue. The feet of the connected field lines, corresponding to the "cusps" in function of local time and latitude, are represented by dots colored (e) in red for SIMU1 and (f) in blue for SIMU2.

[27] Figure 1 shows that the shock is larger in the XZ plane than in the XY plane in both simulations emphasizing an important asymmetry and therefore the limitation of cylindrical symmetry assumption of the shock [*Russell*, 1977; *Slavin and Holzer*, 1981].

[28] In order to compare with MESSENGER observations, simulated BS positions have been fitted separately in the XY and XZ planes, allowing slightly different stand-off distances in XY and XZ planes.

[29] BS asymmetries are generally linked to the IMF orientation [*Trávníček et al.*, 2010; *Fujimoto et al.*, 2007]. In the XY plane, the simulated BS and magnetosphere are slightly more extended in –Y direction because of the negative B_Y component of the IMF (Figures 1a and 1b). XZ plane asymmetry is the consequence of internal magnetic field representation which is an important driver of the structure of the magnetosphere [*Fujimoto et al.*, 2007]. The results show weaker magnetic field intensity in the southern hemisphere in both simulations. This feature can be easily explained for SIMU1 and is a consequence of the Northward shifted dipole. The weak magnetic field region near the South geographic pole in SIMU2 hails from the destructive sum of the dipolar and the quadrupolar fields in this region. As a consequence, the BS and the Magnetosphere are more extended in +Z direction.

[30] Simulated BS positions fits have eccentricities close to 1 and larger SW stand-off distance ($\sim$2.1 R_M) than in the calculations of *Moldovan et al.* [2011] and *Slavin et al.* [2009] ($\sim$1.7 R_M) deduced from MESSENGER observations. Simulated BS crossings both in SIMU1 and SIMU2 are consistent with the dispersion of BS crossings observed by *Moldovan et al.* [2011].

[31] SW parameters are highly variable at Mercury and because of its important orbit eccentricity, the planet undergoes very different average SW conditions [*Sarantos et al.*, 2007]. Magnetosphere and BS dimensions are strongly connected to the upstream environment conditions: in particular, the SW dynamic pressure and the IMF will affect the structure of the Magnetosphere and the different boundary positions [*Fujimoto et al.*, 2007; *Trávníček et al.*, 2007, 2010]. Former simulations predict a paraboloidal-like BS shape with a stand-off distance ranging from the surface to 2.4 R_M [*Kabin et al.*, 2000; *Kallio and Janhunen*, 2003; *Trávníček et al.*, 2007; *Müller et al.*, 2011]. However, these results differ significantly from the results of *Wang et al.* [2010] who suggest a "squashed paraboloid" with a stand-off distance close to 3 R_M. It is worth noticing that MESSENGER reveals a large dynamic of the BS crossings and the simulated BS is well in the range of these BS crossings. SIMU2 predicts a BS position which in better agreement with the average position than SIMU1.

3.2. Comparison With MESSENGER Observations on April 23, 2011

[32] Components of the simulated magnetic field are compared to MESSENGER observations. Without monitoring the key parameters of the SW (particle number densities, velocity and temperature), simulations cannot be performed with the appropriate upstream parameters and reaching a close similarity with MESSENGER measurements is not expected.

[33] Figure 3 displays magnetic field components, in the Mercury Solar Orbital (MSO) coordinates, for the April 23, 2011 MESSENGER orbit between 16:00 and 21:00. Observations and simulations results are compared in Figure 3. To perform this diagnostic a virtual spacecraft is flew in the simulation according to MESSENGER trajectory and simulated magnetic field components are recorded along the trajectory. The projections of MESSENGER trajectory of April 23, 2011, between 16:00 UTC and 21:00 UTC, are displayed on Figure 1. After passing through the southern hemisphere, from 16:00 UTC to 17:00 UTC, MESSENGER reached the northern hemisphere at about 17:00 UTC and the Closest Approach (CA) near the North Pole with an altitude of $\sim$200 km, at 18:00 UTC. Then MESSENGER returned in the southern hemisphere around 18:25 UTC.

[34] Figures 3a–3d represent respectively the total magnetic field, the B_X, B_Y and B_Z components. The color code associated to Figure 3 is the following: black indicates observations, blue SIMU1 solution and red SIMU2 solution.

[35] The simulated magnetic field is globally in good accordance with observations and the general trend is well reproduced in both simulations. The observed and simulated components of the field present many similarities: the B_Z is the dominating component and the sign of the components changes practically at the same time. MESSENGER observed the outbound BS crossings at about 20:10 UTC while SIMU1 and SIMU2 predict a BS crossing respectively at 20:30 UTC (farther from the planet) and 19:50 UTC (closer to the planet). The inbound BS crossings for SIMU1, SIMU2 and observations almost coincide and occurred at $\sim$17:00 UTC.

[36] Before CA, when the virtual spacecraft is in the northern part of the magnetosphere, SIMU1 and SIMU2 mimic the magnetic field profiles observed by MESSENGER along its orbit. Such feature is not surprising since the internal magnetic field for SIMU2 is set up to have a similar representation than SIMU1 in the northern hemisphere. Therefore from the inbound pass a Northward shifted dipole and a combination of centered DQ with adjusted relative coefficient provide a similar solution. After the CA, from 18:20, the magnetic field components of SIMU1 and SIMU2 start to differ, while the virtual spacecraft reaches the southern hemisphere.

[37] The B_{tot} intensity is more important (of $\sim$50 nT) for both simulations than for MESSENGER observations at CA which derives from the B_Z component of the simulated magnetic field and there is a significant discordance between the observations and the two simulations occurring after the closest approach 18:20–19:00/19:10 UTC, mainly due to the simulated B_X component. The simulated southern magnetic lobe seems to have larger magnetic field amplitude than the observations. This feature is also noticed on some of the orbital observations of the magnetic field.

[38] The disagreement between the global model and in situ data can be caused by several factors. *Trávníček et al.* [2007] have illustrated the effect of high and low SW dynamical pressure on Mercury's magnetosphere. Therefore in absence of SW information, the SW density and velocity used in the simulations can differ from SW values that Mercury was facing during the specific time interval and influence the magnetospheric structure. Moreover, although the IMF is quite stable on that date, there is a small variation

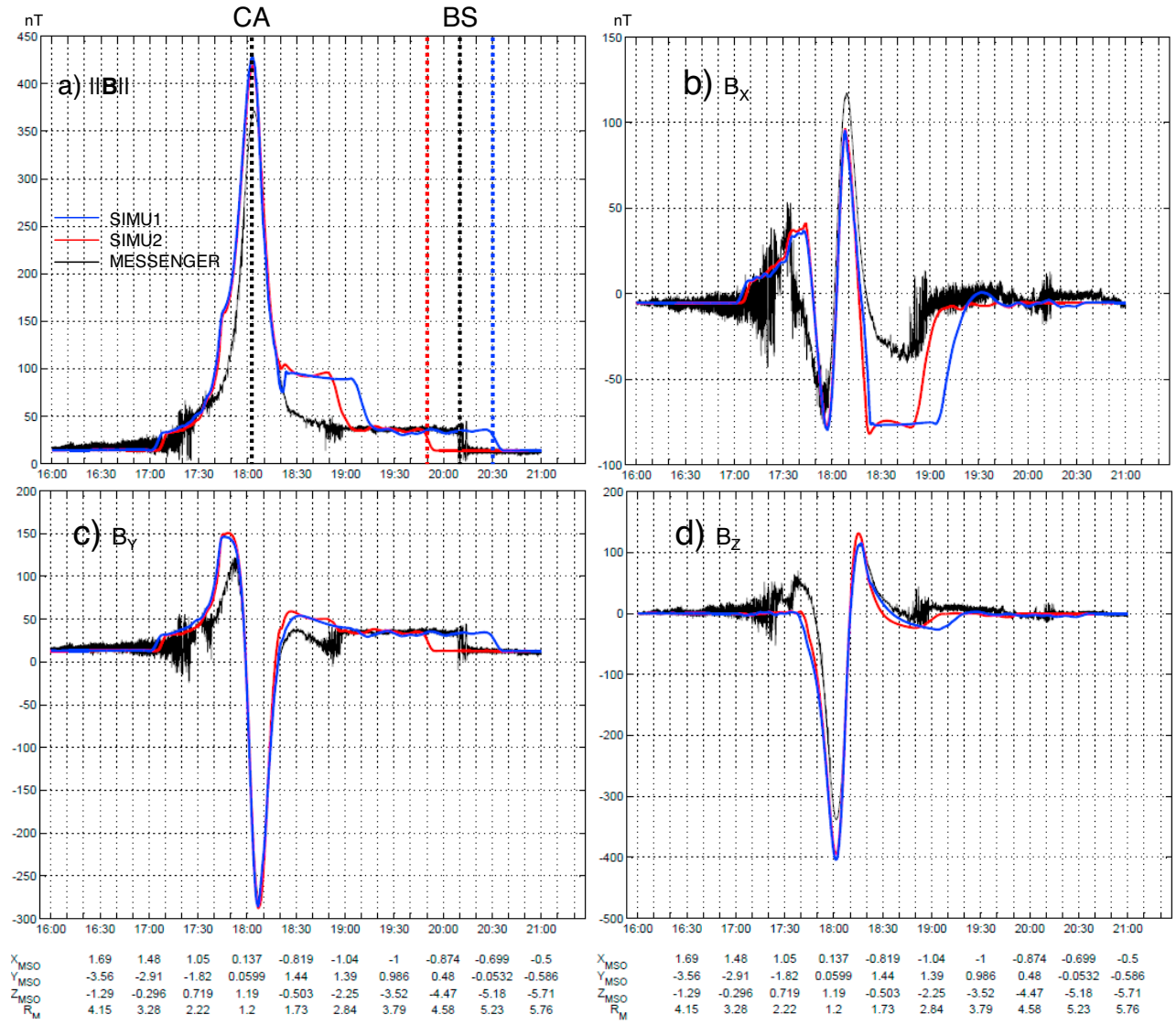

Figure 3. Comparison of the simulated and observed (a) magnetic field intensity and (b–d) components along MESSENGER orbit of April 23, 2011. Simulations results are represented by the blue curve (SIMU1) and the red curve (SIMU2), the magnetic field observed by MESSENGER corresponds to the black curve. The Closest Approach and the BS crossings are indicated in Figure 3a.

of the IMF component (of a few nT) between inbound and outbound (Table 1), larger change of the IMF could occur while MESSENGER was in the magnetosphere and generate a quick reconfiguration, although this scenario is quite unlikely. Despite the assumption that the planetary plasma has a negligible influence on the current, it could have local effects which are missing in this simulation model. Finally, since Mercury's conductivity is assumed to play a role in the closure of the magnetospheric current, a conductive planet may influence the configuration of the magnetosphere [*Janhunen and Kallio*, 2004]. The absence of surface conductivity in the simulation model might result in modifying the electric current circuit in the magnetosphere.

4. Conclusion

[39] Simulations of Mercury's interaction with the SW were performed using a three dimensional parallelized multispecies hybrid model in order to investigate the sensitivity of the Mercury's intrinsic magnetic field representation. Simulations have been run with a northward OD of 484 km and a magnetic moment equal to 196 nT $\times$ R_M^3 (SIMU1) according to *Anderson et al.* [2011], and a combination of dipole and quadrupole magnetic field with adjusted respective coefficients which provide similar magnetic field values than a shifted dipole in northern latitudes higher than 50° (SIMU2).

[40] The main structures of the interaction between the SW and Mercury are well reproduced in the simulations. The results show a detached BS, a magnetosheath, a magnetotail, a neutral current sheet and the "cusps." This study emphasizes numerous discrepancies between the two simulations. In SIMU1, the shock and the magnetosphere are wider than in SIMU2, especially in the southern hemisphere, and the north-south asymmetry apparent in both simulations is increased in SIMU2. The comparison between the simulated

BS, in the two cases, and the average positions of the BS estimated with MESSENGER observations gives a better accordance for SIMU2, mainly in the southern hemisphere. In SIMU2, the magnetosphere is very atypical, presenting a region of closed field lines near the South Pole with a weak magnetic field which is the cause of the important north-south asymmetry. Simulations showed satisfying agreement with MESSENGER observations of the magnetic field on April 23, 2011, though both simulations overestimate the CA magnetic field intensity and the outbound crossing occurs later in SIMU1 and earlier in SIMU2 than in observations. The OD and DQ models imply large differences in the southern magnetosphere although these differences are not entirely reflected along the orbit of MESSENGER. By examining closely the southern magnetosphere and the BS and magnetopause crossings, complementary information could be used to constrain the intrinsic magnetic field properties.

[41] It is worth noticing than the kinetic formalism adopted for this study is not expected to be determinant and similar conclusions could be reached with a 3D (single or multifluid) MHD simulation model. Having already developed hybrid models for small planets and moons like Mars, Titan and Ganymede we have logically adapted our simulation program to Mercury in order to study its magnetosphere where kinetic effects on ions are expected. A similar choice has been made by *Trávníček* [2007], *Kallio and Janhunen* [2003], *Wang et al.* [2010] and *Müller et al.* [2012] Parameters of the SW corresponding to these observations are unknown and an incorrect set of simulation parameters may induce such dissimilarities.

[42] The planetary plasma is not taken into account in the present study. Despite the small density of the magnetospheric plasma, MESSENGER observations reported localized substantial amounts which can locally influence the currents and the plasma pressure. The inclusion of planetary plasma in the model will improve the description of Mercury's magnetosphere.

[43] **Acknowledgments.** Authors thank the NASA's Planetary Data System (PDS), MESSMAGDATA_2001, Vol. MAGMSOSCI1113_V04. Data analysis was done with the AMDA science analysis system provided by the Centre de Données de la Physique des Plasmas (IRAP, Université Paul Sabatier, Toulouse) supported by CNRS and CNES. Research at LATMOS has been partly supported by ANR-CNRS through contract ANR-09-BLAN-223. Authors are indebted to program "Soleil Héliosphère and Magnétosphères" of CNES, the French space administration, for the financial support of their simulation activity.

[44] Masaki Fujimoto thanks the reviewers for their assistance in evaluating this paper.

References

Alexeev, I. I., et al. (2010), Mercury's magnetospheric magnetic field after the first two MESSENGER flybys, *Icarus*, *209*, 23–39, doi:10.1016/j.icarus.2010.01.024.

Anderson, B. J., M. H. Acuña, H. Korth, M. E. Purucker, C. L. Johnson, J. A. Slavin, S. C. Solomon, and R. L. McNutt (2008), The structure of Mercury's magnetic field from MESSENGER's first flyby, *Science*, *321*, 82–85, doi:10.1126/science.1159081.

Anderson, B. J., C. L. Johnson, H. Korth, M. E. Purucker, R. M. Winslow, J. A. Slavin, S. C. Solomon, R. L. McNutt, J. M. Raines, and T. H. Zurbuchen (2011), The global magnetic field of Mercury from MESSENGER orbital observations, *Science*, *333*, 1859–1862, doi:10.1126/science.1211001.

Bida, T. A., R. M. Killen, and T. H. Morgan (2000), Discovery of calcium in Mercury's atmosphere, *Nature*, *404*, 159–161, doi:10.1038/35004521.

Broadfoot, A. L., D. E. Shemansky, and S. Kumar (1976), Mariner 10: Mercury atmosphere, *Geophys. Res. Lett.*, *3*, 577–580, doi:10.1029/GL003i010p00577.

Cargill, P. J., et al. (2005), Cluster at the magnetospheric cusps, *Space Sci. Rev.*, *118*(1–4), 321–366.

Fujimoto, M., W. Baumjohann, K. Kabin, R. Nakamura, J. A. Slavin, N. Terada, and L. Zelenyi (2007), Hermean magnetosphere–solar wind interaction, *Space Sci. Rev.*, *132*, 529–550, doi:10.1007/s11214-007-9245-8.

Glassmeier, K.-H. (1997), The Hermean magnetosphere and its ionosphere-magnetosphere coupling, *Planet. Space Sci.*, *45*, 119–125, doi:10.1016/S0032-0633(96)00095-5.

Janhunen, P., and E. Kallio (2004), Surface conductivity of Mercury provides current closure and may affect magnetospheric symmetry, *Ann. Geophys.*, *22*, 1829–1837, doi:10.5194/angeo-22-1829-2004.

Kabin, K., T. I. Gombosi, D. L. DeZeeuw, and K. G. Powell (2000), Interaction of Mercury with the solar wind, *Icarus*, *143*, 397–406, doi:10.1006/icar.1999.6252.

Kabin, K., et al. (2008), Global MHD modeling of Mercury's magnetosphere with applications to the MESSENGER mission and dynamo theory, *Icarus*, *195*, 1–15, doi:10.1016/j.icarus.2007.11.028.

Kallio, E., and P. Janhunen (2003), Solar wind and magnetospheric ion impact on Mercury's surface, *Geophys. Res. Lett.*, *30*(17), 1877, doi:10.1029/2003GL017842.

Kallio, E., and P. Janhunen (2004), The response of the Hermean magnetosphere to the interplanetary magnetic field, *Adv. Space Res.*, *33*, 2176–2181, doi:10.1016/S0273-1177(03)00447-2.

Killen, R., et al. (2007), Processes that promote and deplete the exosphere of Mercury, *Space Sci. Rev.*, *132*, 433–509, doi:10.1007/s11214-007-9232-0.

Leblanc, F., C. Barbieri, G. Cremonese, S. Verani, R. Cosentino, M. Mendillo, A. Sprague, and D. Hunten (2006), Observations of Mercury's exosphere: Spatial distributions and variations of its Na component during August 8, 9 and 10, 2003, *Icarus*, *185*, 395–402, doi:10.1016/j.icarus.2006.08.006.

Leblanc, F., A. Doressoundiram, N. Schneider, S. Massetti, M. Wedlund, A. López Ariste, C. Barbieri, V. Mangano, and G. Cremonese (2009), Short term variations of Mercury's Na exosphere observed with very high spectral resolution, *Geophys. Res. Lett.*, *36*, L07201, doi:10.1029/2009GL038089.

Massetti, S., S. Orsini, A. Milillo, A. Mura, E. de Angelis, H. Lammer, and P. Wurz (2003), Mapping of the cusp plasma precipitation on the surface of Mercury, *Icarus*, *166*, 229–237, doi:10.1016/j.icarus.2003.08.005.

Massetti, S., S. Orsini, A. Milillo, and A. Mura (2007), Modelling Mercury's magnetosphere and plasma entry through the dayside magnetopause, *Planet. Space Sci.*, *55*, 1557–1568, doi:10.1016/j.pss.2006.12.008.

Matthews, A. P. (1994), Current advance method and cyclic leapfrog for 2D multispecies hybrid plasma simulations, *J. Comput. Phys.*, *112*, 102–116, doi:10.1006/jcph.1994.1084.

McClintock, W. E., E. T. Bradley, R. J. Vervack, R. M. Killen, A. L. Sprague, N. R. Izenberg, and S. C. Solomon (2008), Mercury's exosphere: Observations during MESSENGER's first Mercury flyby, *Science*, *321*, 92–94, doi:10.1126/science.1159467.

McClintock, W. E., R. J. Vernack, E. T. Bradley, R. M. Killen, N. Mouawad, A. L. Sprague, M. H. Burger, S. C. Solomon, and N. R. Izenberg (2009), MESSENGER observations of Mercury's exosphere: Detection of magnesium and distribution of constituents, *Science*, *324*, 610–613.

Milillo, A., et al. (2005), Surface-exosphere-magnetosphere system of Mercury, *Space Sci. Rev.*, *117*, 397–443, doi:10.1007/s11214-005-3593-z.

Modolo, R., and G. M. Chanteur (2008), A global hybrid model for Titan's interaction with the Kronian plasma: Application to the Cassini Ta flyby, *J. Geophys. Res.*, *113*, A01317, doi:10.1029/2007JA012453.

Modolo, R., G. M. Chanteur, E. Dubinin, and A. P. Matthews (2005), Influence of the solar EUV flux on the Martian plasma environment, *Ann. Geophys.*, *23*, 433–444, doi:10.5194/angeo-23-433-2005.

Moldovan, R., B. J. Anderson, C. L. Johnson, J. A. Slavin, H. Korth, M. E. Purucker, and S. C. Solomon (2011), Mercury's magnetopause and bow shock from MESSENGER observations, paper presented at EPSC-DPS Joint Meeting, Eur. Planet. Sci. Congr., Nantes, France.

Müller, J., S. Simon, U. Motschmann, J. Schüle, K. H. Glassmeier, and G. J. Pringle (2011), A.I.K.E.F.: Adaptive hybrid model for space plasma simulations, *Comput. Phys. Commun.*, *182*, 946–966, doi:10.1016/j.cpc.2010.12.033.

Müller, J., S. Simon, Y. C. Wang, U. Motschmann, D. Heyner, J. Schüle, W. H. Ip, G. Kleindienst, and G. J. Pringle (2012), Origin of Mercury's double magnetopause: 3D hybrid simulation study with A.I.K.E.F., *Icarus*, *218*, 666–687, doi:10.1016/j.icarus.2011.12.028.

Ness, N. F., K. W. Behannon, R. P. Lepping, Y. C. Whang, and K. H. Schatten (1974), Magnetic field observations near Mercury: Preliminary results from Mariner 10, *Science*, *185*, 151–160, doi:10.1126/science.185.4146.151.

Ness, N. F., K. W. Behannon, R. P. Lepping, and Y. C. Whang (1975), The magnetic field of Mercury: 1, *J. Geophys. Res.*, *80*, 2708–2716, doi:10.1029/JA080i019p02708.

Ness, N. F., K. W. Behannon, R. P. Lepping, and Y. C. Whang (1976), Observations of Mercury's magnetic field, *Icarus*, *28*, 479–488, doi:10.1016/0019-1035(76)90121-4.

Ogilvie, K. W., J. D. Scudder, V. M. Vasyliunas, R. E. Hartle, and G. L. Siscoe (1977), Observations at the planet Mercury by the plasma electron experiment: Mariner 10, *J. Geophys. Res.*, *82*, 1807–1824, doi:10.1029/JA082i013p01807.

Potter, A., and T. Morgan (1985), Discovery of sodium in the atmosphere of Mercury, *Science*, *229*, 651–653, doi:10.1126/science.229.4714.651.

Potter, A., and T. Morgan (1986), Potassium in the atmosphere of Mercury, *Icarus*, *67*, 336–340, doi:10.1016/0019-1035(86)90113-2.

Potter, A., and T. Morgan (1990), Evidence for magnetospheric effects on the sodium atmosphere of Mercury, *Science*, *248*, 835–838, doi:10.1126/science.248.4957.835.

Potter, A., R. M. Killen, and M. Sarantos (2006), Spatial distribution of sodium on Mercury, *Icarus*, *181*, 1–12, doi:10.1016/j.icarus.2005.10.026.

Raines, J. M., J. A. Slavin, T. H. Zurbuchen, G. Gloeckler, B. J. Anderson, D. N. Baker, H. Korth, S. M. Krimigis, and R. L. McNutt (2011), MESSENGER observations of the plasma environment near Mercury, *Planet. Space Sci.*, *59*, 2004–2015, doi:10.1016/j.pss.2011.02.004.

Russell, C. T. (1977), On the relative locations of the bow shocks of the terrestrial planets, *Geophys. Res. Lett.*, *4*, 387–390, doi:10.1029/GL004i010p00387.

Russell, C. T., D. N. Baker, and J. A. Slavin (1988), The magnetosphere of Mercury, in *Mercury*, edited by F. Vilas, C. Chapman, and M. Matthews, pp. 514–561, Univ. of Ariz. Press, Tucson.

Sarantos, M., R. M. Killen, and K. Danheum (2007), Predicting the long-term solar wind ion sputtering source at Mercury, *Icarus*, *55*, 1584–1595.

Slavin, J. A., and R. E. Holzer (1981), Solar wind flow about the terrestrial planets: 1. Modeling bow shock position and shape, *J. Geophys. Res.*, *86*, 11,401–11,418, doi:10.1029/JA086iA13p11401.

Slavin, J. A., et al. (2008), Mercury's magnetosphere after MESSENGER's first flyby, *Science*, *321*, 85–89, doi:10.1126/science.1159040.

Slavin, J. A., et al. (2009), MESSENGER observations of Mercury's magnetosphere during northward IMF, *Geophys. Res. Lett.*, *36*, L02101, doi:10.1029/2008GL036158.

Trávníček, P., P. Hellinger, and D. Schriver (2007), Structure of Mercury's magnetosphere for different pressure of the solar wind: Three dimensional hybrid simulations, *Geophys. Res. Lett.*, *34*, L05104, doi:10.1029/2006GL028518.

Trávníček, P., P. Hellinger, D. Schriver, D. Hercìk, B. J. Anderson, M. Sarantos, and J. A. Slavin (2010), Mercury's magnetosphere-solar wind interaction for northward and southward interplanetary magnetic field: Hybrid simulation results, *Icarus*, *209*, 11–22, doi:10.1016/j.icarus.2010.01.008.

Vignes, D., C. Mazelle, H. Rme, M. H. Acuña, J. E. P. Connerney, R. P. Lin, D. L. Mitchell, P. Cloutier, D. H. Crider, and N. F. Ness (2000), The solar wind interaction with Mars: Locations and shapes of the bow shock and the magnetic pile-up boundary from the observations of the MAG/ER experiment onboard Mars Global Surveyor, *Geophys. Res. Lett.*, *27*, 49–52, doi:10.1029/1999GL010703.

Vogt, J., B. Zieger, A. Stadelmann, K.-H. Glassmeier, T. I. Gombosi, K. C. Hansen, and A. J. Ridley (2004), MHD simulations of quadrupolar paleomagnetospheres, *J. Geophys. Res.*, *109*, A12221, doi:10.1029/2003JA010273.

Vogt, J., B. Zieger, K.-H. Glassmeier, A. Stadelmann, M.-B. Kallenrode, M. Sinnhuber, and H. Winkler (2007), Energetic particles in the paleomagnetosphere: Reduced dipole configurations and quadrupolar contributions, *J. Geophys. Res.*, *112*, A06216, doi:10.1029/2006JA012224.

Wang, Y.-C., J. Mueller, U. Motschmann, and W. H. Ip (2010), A hybrid simulation of Mercury's magnetosphere for the MESSENGER encounters in year 2008, *Icarus*, *209*, 46–52, doi:10.1016/j.icarus.2010.05.020.

Zurbuchen, T. H., J. M. Raines, G. Gloeckler, S. M. Krimigis, J. A. Slavin, P. L. Koehn, R. M. Killen, A. L. Sprague, R. L. McNutt, and S. C. Solomon (2008), MESSENGER observations of the composition of Mercury's ionized exosphere and plasma environment, *Science*, *321*, 90–92, doi:10.1126/science.1159314.

Zurbuchen, T. H., et al. (2011), MESSENGER observations of the spatial distribution of planetary ions near Mercury, *Science*, *333*, 1862–1865, doi:10.1126/science.1211302.